Missense mutations in the ABCB6 transporter cause dominant familial pseudohyperkalemia

Immacolata Andolfo,[1,2] Seth L. Alper,[3,4,5] Jean Delaunay,[6] Carla Auriemma,[1,2] Roberta Russo,[1,2] Roberta Asci,[1] Maria Rosaria Esposito,[1] Alok K. Sharma,[3,4,5] Boris E. Shmukler,[3,4,5] Carlo Brugnara,[7] Lucia De Franceschi,[8] and Achille Iolascon[1,2]*

Familial Pseudohyperkalemia (FP) is a dominant red cell trait characterized by increased serum [K^+] in whole blood stored at or below room temperature, without additional hematological abnormalities. Functional gene mapping and sequencing analysis of the candidate genes within the 2q35–q36 critical interval identified—in 20 affected individuals among three multigenerational FP families—two novel heterozygous missense mutations in the *ABCB6* gene that cosegregated with disease phenotype. The two genomic substitutions altered two adjacent nucleotides within codon 375 of ABCB6, a porphyrin transporter that, in erythrocyte membranes, bears the Langereis blood group antigen system. The ABCB6 R375Q mutation did not alter the levels of mRNA or protein, or protein localization in mature erythrocytes or erythroid precursor cells, but it is predicted to modestly alter protein structure. ABCB6 mRNA and protein levels increase during *in vitro* erythroid differentiation of $CD34^+$ erythroid precursors and the erythroleukemia cell lines HEL and K562. These data suggest that the two missense mutations in residue 375 of the ABCB6 polypeptide found in affected individuals of families with chromosome 2-linked FP could contribute to the red cell K^+ leak characteristic of this condition. Am. J. Hematol. 88:66–72, 2013. © 2012 Wiley Periodicals, Inc.

Introduction

Familial pseudohyperkalemia (FP) is a dominant red cell trait characterized by increased serum [K^+] measured in whole-blood specimens stored at or below room temperature. This dominantly inherited trait is not accompanied by clinical symptoms or biological signs except for borderline abnormalities of red cell shape [1]. FP Lille was described in a large family of Flemish origin with morphologically normal red cells [2,3]. In this family, cation leak measured *in vitro* in the presence of ouabain and bumetanide showed normal K^+ efflux at 37°C, which increased greatly at 22 and 9°C [3]. The subsequently reported asymptomatic cases of FP Chiswick and FP Falkirk [4] were remarkable for increased MCV. FP Lille was mapped to 2q35–q36 by genome-wide search [5].

FP is considered as a subtype of the larger group of leaky red blood cell (RBC) disorders that include Southeast Asian ovalocytosis [6], dehydrated hereditary stomatocytosis (DHSt) [7], overhydrated hereditary stomatocytosis (OHSt) without or with neurological symptoms [8], and cryohydrocytosis (CHC). There appears to be a continuum between FP and DHSt that may be associated with pseudohyperkalemia [7]. Several temperature-dependent patterns of cation leak have been characterized in these conditions by measurements of ^{86}Rb influx insensitive to ouabain and bumetanide [9]. FP stands out among the leaky RBC disorders for its mild clinical and hematological phenotype and its minimal changes in cell shape.

Mutations in several genes have been shown to cause red cell cation leak disorders. These include *SLC4A1* (an ion exchange) in CHC and in atypical forms of hereditary spherostomatocytosis [10,11], *RHAG* (Rh-associated glycoprotein) in isolated stomatin-deficient OHSt [12,13] *GLUT1* (glucose transporter 1) in echinocytosis with paroxysmal dyskinesia [14], stomatin-deficient cryohydrocytosis [15] or in CHC [16] or pseudohyperkalemia and hemolysis [17] with neurological symptoms, and *PIEZO1* (mechanosensitive cation channel protein FAM38A) in DHSt [18]. These findings suggest that distinct missense mutations in various red cell membrane solute transporters or channels generate cation leak pathways either through the mutant proteins themselves or by deregulating one or more independent cation permeabilities of the red cell membrane.

Here, we report that in FP Lille, linked to chromosome 2q, and in two other FP families, the causal mutations reside in the same codon (375) of the ABCB6 gene, encoding the ABCB6 polypeptide reported to be a porphyrin transporter [19]. This protein was recently identified in the RBC membrane [20], where it displays the Langereis blood group [21].

Materials and Methods

Cases reports. FP Lille was first diagnosed in a mother and daughter [2,3] from a large family of Flemish descent. The carriers were hematologically normal. Temperature-dependent ^{86}Rb influx showed a shallow slope pattern [5]. The responsible gene was mapped to 2q35–q36 (very close to marker D2S1338), based on the analysis of 23 carriers (including the above-mentioned daughter as individual II.8)

[1]CEINGE, Biotecnologie Avanzate, Naples, Italy; [2]Department of Biochemistry and Medical Biotechnologies, "Federico II" University of Naples, Naples, Italy; [3]Division of Nephrology, Beth Israel Deaconess Medical Center, Boston, Massachusetts; [4]Division of Molecular and Vascular Medicine, Beth Israel Deaconess Medical Center, Boston, Massachusetts; [5]Department of Medicine, Harvard Medical School, Boston, Massachusetts; [6]UMR_S 779, INSERM, Faculté de Médecine Paris-Sud, Université Paris-Sud, 94275 Le Kremlin-Bicêtre, Paris, France; [7]Department of Laboratory Medicine, Children's Hospital Boston, and Harvard Medical School, Boston, Massachusetts; [8]Department of Medicine, University of Verona, Piazzale Lo Scuro 10, Verona, Italy

Additional Supporting Information may be found in the online version of this article.

Conflict of interest: Nothing to report

*Correspondence to: Achille Iolascon, CEINGE Biotecnologie Avanzate, Via Gaetano Salvatore, 486, Naples 80145, Italy. E-mail: achille.iolascon@unina.it

Contract grant sponsor: Italian Ministero dell'Università e della Ricerca (MIUR); Contract grant sponsor: Telethon (Italy); Contract grant number: GGP09044, MUR-PS 35-126/Ind; Contract grant sponsor: Regione Campania, DGRC 1901/200; Contract grant sponsor: The Doris Duke Charitable Foundation.

Received for publication 17 October 2012; Accepted 17 October 2012

Am. J. Hematol. 88:66–72, 2013.

Published online 25 October 2012 in Wiley Online Library (wileyonlinelibrary.com). DOI: 10.1002/ajh.23357

versus 11 noncarriers [5]. In 2011, the daughter's RBC indices were RBC = 4.5 T/L, hemoglobin = 13.7 g/dL, hematocrit = 42.6%, MCV = 96.0 fL, MCH = 30.7 pg, and MCHC = 32.2 g/dL. All RBC indices were normal except for the slightly elevated MCV. Eleven carriers and seven noncarriers from the FP Lille family were investigated in this study.

FP Falkirk was previously described in a family of Pakistani origin [4,22]. The hematologic indices were normal, but macrocytosis was noted after 24-hr storage on ice. ^{86}Rb influx measurement as a function of temperature showed a shoulder pattern [4], at variance with FP Lille. This study investigated four carriers and one noncarrier from this family.

FP "East London" was first diagnosed in a Bangladeshi family [23]. Carriers showed high plasma [K^+] values and anemia, and were considered nonhemolytic owing to the absence of reticulocytosis or jaundice [7]. ^{86}Rb influx measurement as a function of the temperature showed a shoulder pattern slope [23], as in FP Falkirk. This study investigated five carriers and six noncarriers from this family.

Patients and sequencing analysis. Blood was obtained for genetic analysis from affected and unaffected family members, and from healthy controls, after signed informed consent, according to the Declaration of Helsinki. Blood collection was approved by local university ethics committees.

Genomic DNA was prepared from peripheral blood with the Wizard Genomic DNA purification kit (Promega, Milano, Italy). The search for mutations was performed by direct sequencing, using 75-ng genomic DNA. All exons and flanking splice junctions of the *ABCB6* gene were amplified by PCR in a 25 μL volume with Master Mix 2X. Oligonucleotide primers were designed by the program Primer3 v.0.4.0. Primer sequences are available on request. The integrity of PCR products was checked by agarose gel electrophoresis. Direct sequencing was performed using the BigDye® Terminator Cycle Sequencing Kit (Applied Biosystems, Branchburg, NJ) and a 3730 DNA Analyzer (Applied Biosystems). Missense substitution mutations in ABCB6 (Q9NP58) were evaluated by the PolyPhen2 program [24].

Reticulocyte isolation. Reticulocytes were isolated from peripheral blood of II.8 patient and healthy controls according to a previously described protocol [25].

RNA isolation and cDNA synthesis from CD34$^+$ cells. Total RNA was isolated [26] from $CD34^+$ cells at days 0, 7, and 14 of erythroid differentiation. Single-strand cDNA was synthesized from 2 μg RNA template, using 2.5 units VILO reverse transcriptase (Life Technologies, Monza, Italy), and 2.5 μM oligo-dT as primer, in a total final volume of 20 μL.

Bioinformatic modeling of ABCB6 protein structure. Three-dimensional (3D) structural models were generated of homodimeric human WT ABCB6 and of the corresponding regions of the two mutant ABCB6 polypeptides R375Q and R375W. The ABCB1A/MDR1a multidrug transporter protein of *Mus musculus* (RCSB PDB ID 3G5U) served as a reference template for the inward-facing conformation of ABCB6. For inward conformation modeling, ABCB6 amino acid sequences (Uniprot Q9NP58) encompassing residues 237–826 and residues 246–826 were aligned onto the structurally characterized mABCB1A sequences of Val33-Thr626 and Leu684-Ala1271, respectively. The Sav1866 ABC transporter of *Staphylococcus aureus* (RCSB PDB ID 2HYD) served as a reference template for the outward-facing conformation of ABCB6. Outward conformational modeling of ABCB6 aligned ABCB6 residues 248–827 onto the structurally characterized sequence of Sav1866 (Met1-Leu578).

Sequences were aligned using the program ClustalW2. The aligned ABCB6 sequences were manually adjusted to redefine secondary structural regions as predicted by PSIPRED. MODELLER v9.9 [27] was used to generate 100 structural models of each of the above-defined regions of WT ABCB6 and the two mutant proteins, in both inward- and outward-facing conformations. The best five structural models of each polypeptide with lowest objective function values (as implemented in MODELLER) were subjected to energy minimization in GROMACSv4.5.4 [28]. Structural models were converged using steepest-descent energy minimization with 1,000 steps of step size 0.01 nm. The stereochemical quality of each energy-minimized structure was assessed by PROCHECK [28a]. The average of three models of highest stereochemical quality was chosen to represent the ABCB6 structural model for each inward- and outward-facing conformation. 3D structural models were visualized and aligned using MolMol [29] and PyMOL (Molecular Graphics System, Version 1.5.0.4 Schrödinger, LLC). Figures were prepared in PyMOL. Note that each modeled dimeric ABCB6 polypeptide lacks its "M0" region comprising the putative ecto-N-terminal segment and the first five N-terminal-proximal transmembrane helices. This M0 region, for which no structural template is available, is otherwise present only in seven ABCC proteins [30].

Results

Evaluation of FP critical region candidate genes

To find the causative gene for dominantly inherited FP linked to 2q35–q36, we applied a functional screening method to the genes located in the critical region mapped by Carella [5] (D2S301–D2S163; Supporting Information Fig. 1A). We focused on 28 genes divided into functional categories as transporters, ion channels, and surface receptors (Supporting Information Fig. 1B). To reduce the number of genes to be evaluated, we filtered with gene expression information from Unigene (NCBI http://www.ncbi.nlm.nih.gov/unigene) and Genecard (Weizmann Institute of Science http://www.genecards.org/). Finally, we integrated the publicly available data with experimental expression data on $CD34^+$ cells during erythroid differentiation. We selected *ABCB6* as a candidate gene based on its elevated expression in blood and bone marrow and its increased expression during erythroid differentiation (data not shown). The encoded ABCB6 protein is involved in porphyrin transport [19] and was recently identified in the RBC membrane [20].

ABCB6 mutational analysis

We sequenced the ABCB6 gene in 20 affected FP patients and 14 nonaffected family members from three affected families. Pedigrees are shown in Supporting Information Fig. 2 for FP Lille [5], for FP Falkirk [4], and for FP East London [23]. In FP Lille family, we analyzed 11 individuals and found the heterozygous mutation c.1124 G > A, p.R375Q (Fig. 1) in seven affected subjects. The mutation was absent in the four healthy subjects of the same family. In family FP Falkirk, we found the heterozygous mutation, c.1123 C > T, p.R375W in four affected subjects (shown in the exon–intron diagram, Fig. 1A). No mutation was found in one unaffected subject tested in this family. The heterozygous mutation in family FP East London in five affected subjects was identical to that in FP Falkirk, c.1123 C > T, p.R375W. No mutation was found in the six unaffected subjects of this family. The two different mutations were associated with distinct temperature-dependent patterns of erythrocyte cation leak. Thus, erythrocytes from affected individuals with FP Lille (p.R375Q) exhibited a shallow slope curve, whereas erythrocytes from affected individuals with FP Falkirk and FP East London (p.R375W) exhibited a shoulder-shaped curve. None of the carriers exhibited abnormalities of the iris or retina. The recessive, loss-of-function mutations associated with the Lan (−/−) blood group were not present in FP individuals.

The two genomic mutations, encoding substitutions of two adjacent nucleotides within the same codon, produce different missense changes in the same amino acid residue (Arg 375), as shown in Fig. 1A,B. Neither nucleotide change was present in the 1,000 genomes database, or in 50 healthy subjects (unrelated to the three families analyzed). Amino acid residue R375 of ABCB6 is conserved among all species analyzed (Fig. 1C). The two missense mutations found in our three FP families each have PolyPhen2 scores (http://genetics.bwh.harvard.edu/pph2/index.shtml) of 1.000 (probably damaging).

Structural Modeling of wild-type and mutant ABCB6

To assess the potential effects of the identified mutations on protein structure, we generated 3D structural models of (putatively dimeric) human WT ABCB6 residues 231–827 (Fig. 2) and the corresponding regions of the two mutant ABCB6 polypeptides R375Q and R375W (Supporting Information Figs. 3 and 4), using as reference templates for the inward-facing conformation the crystal structure of

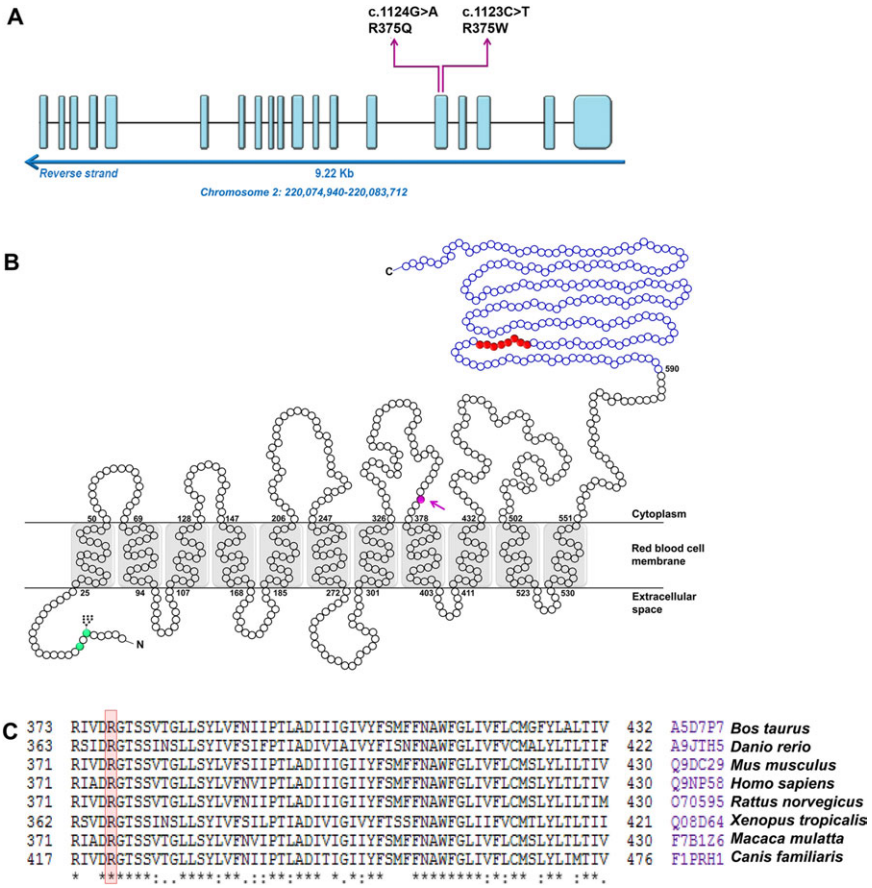

Figure 1. Mutations analysis. A. Diagram showing *ABCB6* gene sequence (blue square: exons, black bars: introns); the arrows indicate the single codon which has undergone two missense substitutions in three families previously mapped to chromosome 2q (Left: FP Lille; Right: FP Falkirk and FP East London) Nucleotide numbering reflects cDNA numbering with +1 corresponding to the A of ATG translation initiation codon in the reference sequence (Ensembl transcript ID ENST00000265316). The initiation codon is codon 1. B. Schematic representation of the two-dimensional structure of ABCB6 in the RBC membrane, based on the experimentally supported structure of Fukuda [47]. Circles represent individual amino acid residues. The arrow indicates the ABCB6 residue mutated in the three FP families. Gray boxes depict putative transmembrane domains (with residue numbers above and below indicating HMMTOP-predicted transmembrane domain boundaries). Amino acids of the nucleotide-binding domain (NBD, blue circles) include those directly involved in ATP binding (red circles). The purple circle is the mutated amino acid in the three families studied here. Green circles are consensus *N*-glycosylation sites, only one of which (branched glycan symbol at residue 6) is experimentally validated by Fukuda [47]. C. Evolutionary conservation of mutated residue Arg 375 (red box), across the species indicated at right (with Uniprot codes).

M. musculus ABCB1A/MDR1, a multidrug transporter protein (RCSB PDB ID 3G5U) [31], and for the outward-facing conformation the crystal structure of *S. aureus* ABC transporter Sav1866 (RCSB PDB ID 2HYD) [32]. Arg 375 is highlighted in blue in both inward-facing and outward-facing models. This site of FP missense mutations is situated at or close to the cytoplasmic surface of the lipid bilayer, below the proposed substrate binding site (red webbing) in the inward conformation form of the protein, with the guanidinium groups of the two monomers well separated (Fig. 2A). In the modeled outward-facing conformation, Arg 375 lies adjacent to or within the proposed ABCB6 intermonomeric substrate binding region, with the guanidinium NH2 atoms of each monomer's R375 residue separated by 5.5 Å only (Figs. 2B,C). Within the modeled dimer, the intermonomeric separations between side-chain amide nitrogens of mutant 375Q and between side-chain indole nitrogens of mutant 375W are modeled as larger, between 6.5 and 7.7 Å (data not shown), but the large structural differences between the modeled inward and the outward conformations of ABCB6 are minimally affected by the FP mutant missense substitutions (Supporting Information Figs. 3 and 4). Both mutations are predicted to produce modest changes in global protein structure as shown by the regions of slightly divergent alignment of the WT and mutated proteins, slightly larger in the inward than in the outward conformations (Supporting Information Figs. 3 and 4).

ABCB6 expression in blood and red cells of affected and unaffected subjects

ABCB6 mRNA expression in blood was indistinguishable between affected individual II.8 and unaffected subject III.10 from FP Lille family [4] and the four other unrelated healthy subjects (Fig. 3A). ABCB6 protein expression in red cells of affected individual II.8 was also equivalent to that in healthy controls, as judged by immunoblot (Fig. 3B). ABCB6 localization in RBCs was evaluated in patient II.8. Confocal microscopy analysis showed that ABCB6 was expressed at the RBC membrane, and colocalized in some membrane regions with CD55 (Decay Accelerating Factor bearing the Cromer blood group system) (Fig. 3C), in agreement with the recently published results [21]. We further confirmed ABCB6 localization in the red cell membrane by substantial colocalization with glycophorin A in control red cells (Fig. 3D) (for a negative control of ABCB6 red cell immunostaining, see Supporting Information Fig. 5A). Thus, mutant R375Q–ABCB6 is expressed at normal levels and is localized normally in the mature red cell membrane in 2q FP Lille.

ABCB6 expression during erythroid differentiation

The previous results demonstrated that ABCB6 is expressed in RBCs and during erythroid differentiation of K562 cells [20,21]. We examined ABCB6 expression and localization in an *ex vivo* model of erythroid differentiation. $CD34^+$ hematopoietic precursors induced to erythroid

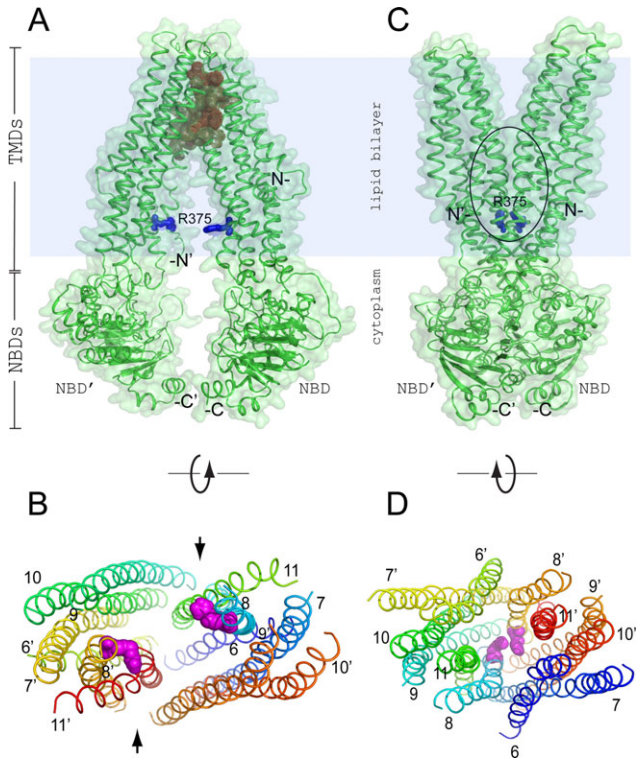

Figure 2. 3D structure models of ABCB6 in inward conformation. A. 3D structural model of homodimeric WT human ABCB6 protein in an inward-facing conformation, as modeled on the aligned structure of *M. musculus* ABCB1A (PDB ID 3G5U; see **Materials and Methods** section). Monomer "a" represents ABCB6 aa residues 246 (N-) to 826 (-C) modeled on the transmembrane helices 1–6 and NBD1 of ABCB1A. Monomer "b" represents ABCB6 aa residues 237 (N′-) to 826 (-C′) modeled on ABCB1A transmembrane helices 7–12 and NBD2. A space-filling model (light green) is superimposed on the modeled polypeptide backbone ribbon structure (dark green). Arg375 (highlighted in blue) is located between the membrane-spanning helices and the NBDs, extending into the cytoplasmic vestibule of the dimer. The cavity (red webbing) at the intermonomeric interface outlines a postulated intramembranous binding site for inhibitors of ABCB6-mediated porphyrin transport [48] corresponding to the ABCB1 binding site of inhibitor QZ59 [31]. B. Transverse intramembranous profile of the modeled inward-facing conformation of dimeric ABCB6, with transmembrane helices rotated (around the axis shown) 90° away from the reader. The view, lacking NBDs, is from the cytoplasmic edge of the inner leaflet, near the separated Arg375 residues (magenta), looking outward. The colored M1 domain helices are numbered 6–11 for ABCB6 monomer "a," and 6′–11′ for monomer "b" of the ABCB6 dimer. Helices are labeled at ends closest to the reader. The arrows between helices 9 and 11 on one side, and helices 9′ and 11′ on the other side of the dimer mark the locations of side apertures proposed in mouse ABCB1 to mediate hydrophobic drug uptake from the inner leaflet of the lipid bilayer for subsequent efflux from the cell, or for flippase-like transfer to the outer leaflet. C. 3D structural model of homodimeric WT human ABCB6 protein in an outward-facing conformation, as modeled on the aligned structure of *S. aureus* Sav1866 (PDB ID 2HYD). The black oval encloses a central cavity at the intermonomeric interface, hypothesized to be an intramembranous substrate binding site (as predicted for homodimeric Sav1866 of *S. aureus*) [32]. Note that each ABCB6 monomer lacks its ectofacial N-terminal tail and putative transmembrane spans 1–5, but includes putative transmembrane spans 6–11 (TM) followed by the single-nucleotide-binding domain (NBD). D. Transverse intramembranous profile of the modeled outward-facing conformation of dimeric ABCB6, with the transmembrane helices rotated (around the axis shown) 90° toward the reader. The view, lacking NBDs, is from the edge of the outer leaflet looking inward toward the approximated Arg 375 residues (magenta) near the cytoplasmic face of the inner leaflet. Helices are labeled at ends closest to the reader.

differentiation with 14-day erythropoietin treatment, as detailed in **Materials and Methods** section. We analyzed ABCB6 mRNA expression during erythroid differentiation on day 7, the stage of proerythroblast expansion and maturation, and on day 14, when most cells resemble late-stage erythroblasts. As shown in Fig. 4A, ABCB6 mRNA was significantly upregulated after 14 days of erythropoietin treatment ($P = 0.002$). These data were confirmed at the protein level by Western blotting (Fig. 4B).

We analyzed the expression of ABCB6 mRNA and protein in two additional *in vitro* cellular models widely used to study hematopoietic cell growth and differentiation: HEL cells and K562 cells. The HEL and K562 cells were differentiated through the erythroid lineage with hemin for 6 days, as described in **Materials and Methods** section. In HEL cells, ABCB6 mRNA levels increased after 4 days of differentiation and remained stable at 6 days (Supporting Information Fig. 6A). These data were confirmed at the protein level by immunoblot (Supporting Information Fig. 6B). In K562 cells, ABCB6 mRNA levels increased gradually at 7 and 14 days (Supporting Information Fig. 6C), in parallel with gradual increases in protein levels detected by immunoblot (Supporting Information Fig. 5D). Confocal microscopy analysis showed that ABCB6 was expressed on the RBC membrane of $CD34^+$ cells during erythroid differentiation and colocalized with the membrane marker CD55 in some membrane regions (Fig. 4C).

Discussion

We have identified two missense mutations in residue 375 of the ABCB6 transporter that cause FP, a dominant red cell trait characterized by an increase of serum [K^+] detectable only after *ex vivo* storage of whole blood at room temperature or in the cold, in the absence of any other hematological abnormality. The responsible gene in FP Lille was previously mapped to 2q35–36. *ABCB6* was selected as a strong candidate gene within the critical region based on its expression in $CD34^+$ cells during erythroid differentiation. Affected individuals in FP Lille exhibited the c.1124 G > A, p.R375Q mutation in *ABCB6*. Affected subjects in FP Falkirk and FP East London families exhibited the *ABCB6* mutation c.1123 C > T, pR375W affecting the same codon.

ABCB6 belongs to the family of ATP-binding cassette (ABC) transporters, one of the most abundant families of integral membrane proteins [33]. The ABC transporters couple ATP binding and hydrolysis to the transport of endogenous and xenobiotic substrates across cellular membranes. ABCB6 is a member of the B (MDR/TAP) subfamily of ABC transporters best known as drug-resistance genes, and it can form homodimers [19]. Indeed, increased ABCB6 expression correlates with increased drug resistance in multiple cell lines [34,35]. A specific ABCB6 function was first described in *Saccharomyces cerevisiae* mutants lacking mitochondrial ABC transporter *Atm1p* [36]. Complementation of Atm1p-deficient yeast with human ABCB6 rescued the phenotypic alterations, leading to the proposal that *ABCB6* is the human ortholog of *Atm1p* [36]. In 2006, ABCB6 was shown to catalyze mitochondrial uptake of coproporphyrin III, as an important regulator of cellular porphyrin biosynthesis [19]. However, Tsuchida [37] questioned the mitochondrial localization of ABCB6, providing evidence for its localization in endoplasmic reticulum and Golgi membranes, rather than in mitochondria. The observation of extra-mitochondrial localization has been extended by the study of dominantly inherited ABCB6 mutations in patients with ocular coloboma [38].

Gene expression profiling studies of zebrafish blood formation mutants revealed ABCB6 among genes of the erythroid cluster [39]. ABCB6 was recently shown to carry the Lan (Langereis) blood group antigen system of the RBC plasma membrane [21]. The asymptomatic Lan (−/−) carriers display a variety of recessive null mutations, all with red cells of normal phenotype [21]. Lan blood group mismatch can cause hemolytic transfusion reactions and hemolytic disease of the newborn. Kiss [20] recently confirmed ABCB6 as a glycoprotein present in the membrane of mature erythrocytes and in exosomes released from re-

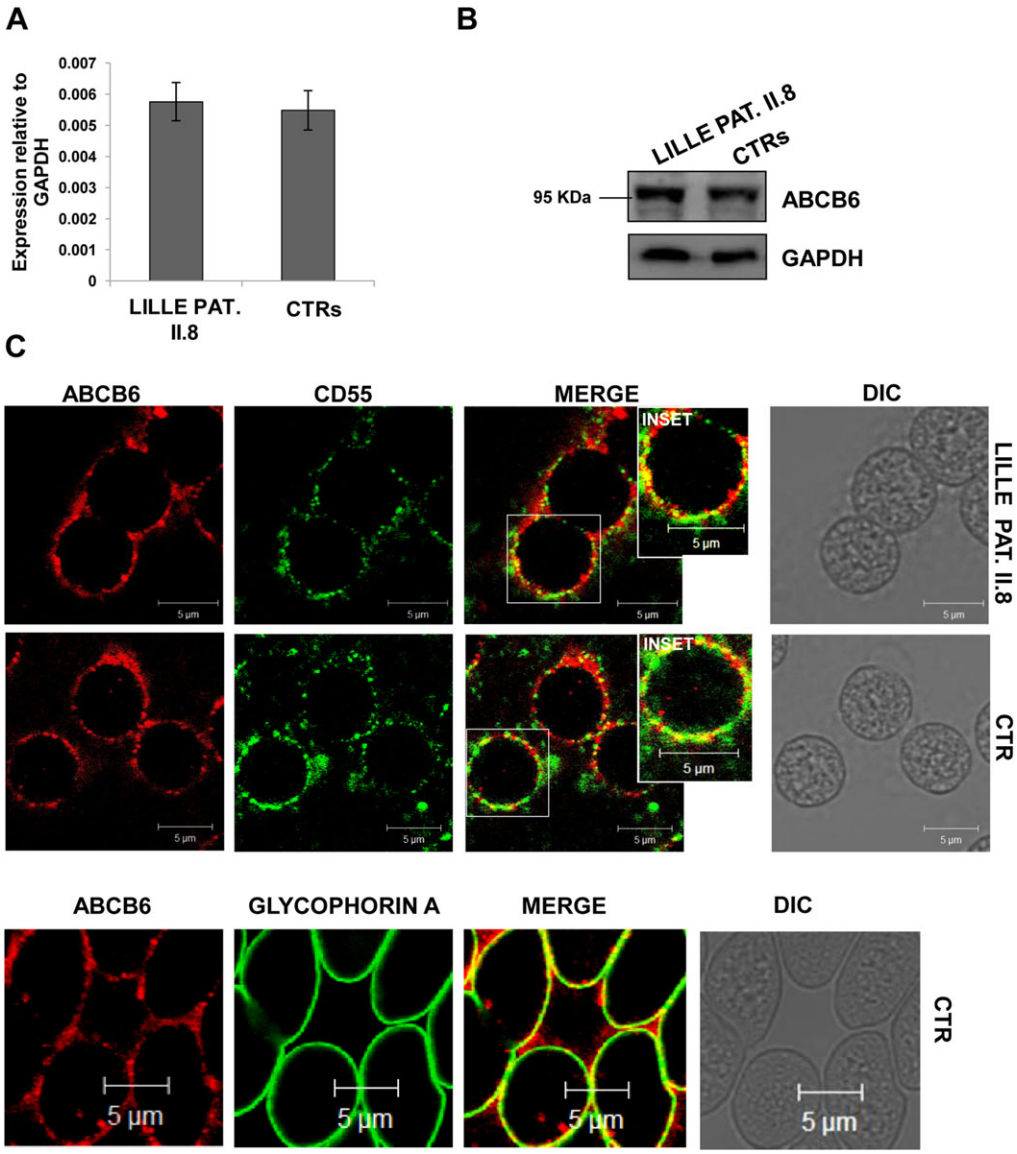

Figure 3. Characterization of ABCB6 in patient's RBCs. A. ABCB6 mRNA levels in peripheral blood samples of Lille patient II.8 and control subjects (pool of four subjects). Values are means ± s.e.m. of three independent experiments. B. Immunoblot showing ABCB6 protein expression in RBC membrane of Lille patients II.8 and from the four pooled control subjects. GAPDH is loading control. One of the two similar experiments. C. Laser-scanning confocal microscopy images of RBCs smear of Lille patients II.8 and control samples analyzed by immunofluorescence with ABCB6 rabbit polyclonal antibody (red) and CD55 (membrane marker, green) showing the merge of the two signals (Rr = 0.44, R = 0.79 for Lille patient II.8; Rr = 0.15, R = 0.48 for control sample). D. Laser-scanning confocal immunofluorescence microscopy images of a control RBC smear costained with rabbit polyclonal antibody to ABCB6 (red) and mouse monoclonal antibody to glycophorin A (membrane marker, green) showing the merge of the two signals (Rr = 0.60, R = 0.79). DIC indicating the differential interference contrast to demonstrate the presence of the RBCs. Cells were imaged with a Zeiss LSM 510 metaconfocal microscope equipped with a 1.4 NA oil immersion plan Apochromat 100× objective. Luminosity and contrast were adjusted using the Axiovision software. Representative of three independent experiments.

ticulocytes during the final steps of erythroid maturation. Knockdown studies demonstrated that ABCB6 function is not required for *de novo* heme biosynthesis in differentiating K562 cells, excluding this ABC transporter as an essential regulator of porphyrin synthesis. We confirm that ABCB6 is upregulated during erythroid differentiation and is localized at the plasma membrane in mature RBCs and in $CD34^+$ during the erythroid differentiation (Figs. 3 and 4).

Abcb6$^{-/-}$ mice exhibit a grossly normal phenotype, but lack ATP-dependent mitochondrial uptake of coproporphyrin III. ABCB6 deficiency upregulates heme and iron pathways that are necessary for normal development. However, in conditions of extreme demand for porphyrins (such as during phenylhydrazine stress), these adaptations appear inadequate, suggesting the importance of ABCB6 for optimal survival under these stress conditions [40].

The FP mutation site encoding ABCB6 Arg 375 is a CpG sequence, the usual context of human mutational hotspots, in which C > T and G > A mutations likely result from deamination of methylated cytosine [41]. The FP mutations did not alter mRNA or protein abundance, as shown in the FP Lille subject (Fig. 3). However, the mutations could affect ABCB6 protein structure or conformational dynamics. Arg 375 is predicted to reside at or near the junction of cytoplasmic loop 4 and the inner leaflet portion of transmembrane helix 8 of ABCB6 (Figs. 1B and 2). The residue lies within a conserved RGT sequence in which the β3 integrin cytoplasmic domain contributes to outside-in signaling [42]. The corresponding residue N186 of the cystic fibrosis transmembrane regulator (CFTR/ABCC4) has been modeled to contribute to a hydrophilic ring surrounding the enlarging cytoplasmic vestibule of the CFTR anion translo-

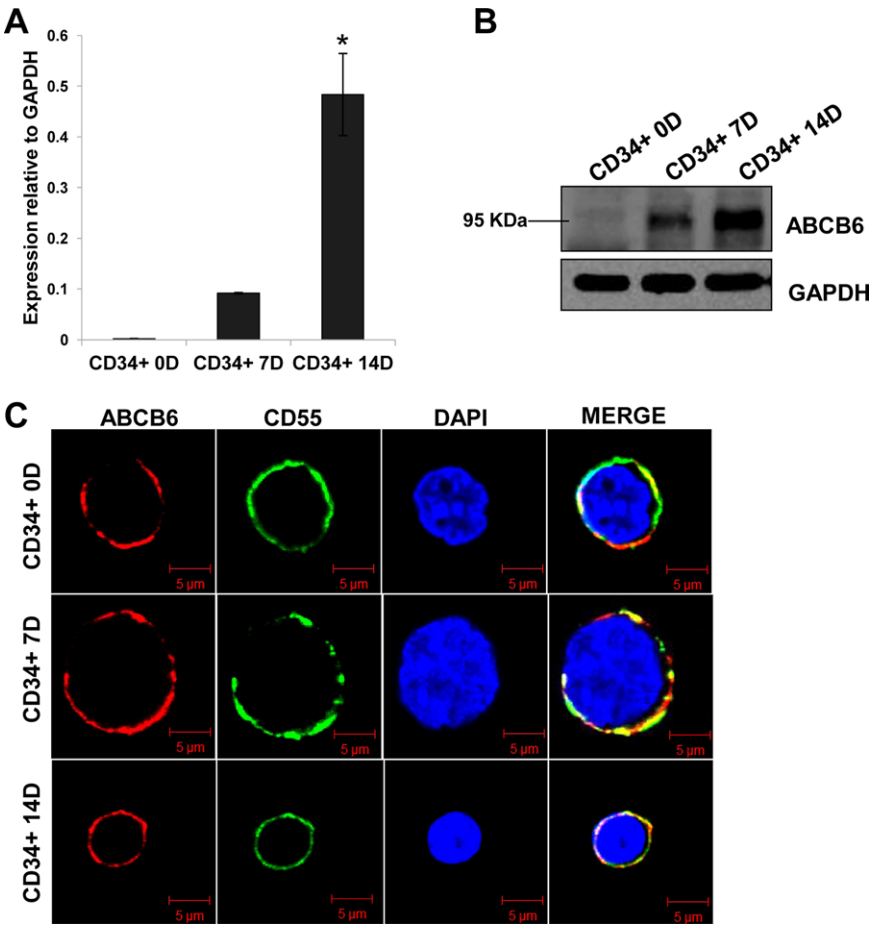

Figure 4. ABCB6 expression and localization in CD34$^+$ during erythroid differentiation. A. ABCB6 mRNA levels (normalized to GADPH) in CD34$^+$ cells induced to erythroid differentiation by EPO at 0, 7, and 14 days by qRT-PCR. **P-value 0.02* (CD34$^+$ 14D vs. CD34$^+$ 7D). B. Immunoblot of ABCB6 protein in CD34$^+$ cells induced to erythroid differentiation at 0, 7, and 14 days using Western blots. GAPDH serves as loading control (one of the two similar experiments). C. Laser-scanning confocal immunofluorescence microscopy images of CD34$^+$ cells induced to differentiation by EPO, showing the merge of the two signals ABCB6 (red) and CD55 (green) (Rr = 0.66, R = 0.89 for CD34$^+$ at day 0; Rr = 0.35, R = 0.40 at day 7; Rr = 0.74, R = 0.71 for CD34$^+$ at day 14). Cells were imaged with a Zeiss LSM 510 metaconfocal microscope equipped with a 1.4 NA oil immersion plan Apochromat 63× objective. Luminosity and contrast were adjusted using the Axiovision software. Representative of three independent experiments.

cation pathway [43]. The CFTR mutation N186K encoding a likely loss-of-function variant has been found in a compound heterozygous cystic fibrosis patient in trans with the most common loss-of-function mutation ΔF508 (ID:3215 at www.umd.be/CFTR) [44].

Our models of ABCB6 structure predict small distortions by FP mutations at residue 375 in both the transmembrane spans and the NBD. Arg 375 is modeled near a postulated substrate-binding site and perhaps along the substrate translocation pathway of ABCB6 in the outward-facing conformation. In view of the modeled intermonomeric proximity of the two Arg 375 residues, the FP missense mutations at this site might modify the rigid body motions proposed for transmembrane domain cytoplasmic loops during the ATP hydrolysis-driven transport conformational cycle [45], or otherwise impede the transport cycle. These changes could lead either to cation leak through the normal substrate translocation pathway of ABCB6, or to the generation of a novel constitutive or cyclic leak pathway through the protein. Alternatively, mutant ABCB6 polypeptides could activate an independent cation permeability through direct or indirect protein–protein interaction, as proposed for CHC mutations in AE1/SLC4A1 [11,15], stomatin-deficient OHSt mutations in RhAG [12,13], and suggested by the fourfold elevation of K–Cl cotransport observed in red cells of patient FP Lille (LdeF, unpublished data).

ABCB6 mutations cause at least three phenotypically disparate diseases: ocular coloboma, Lan (−/−) group, and FP. The absence of the ABCB6 protein, as in individuals with the Lan (−/−) blood group, is associated, in addition to loss of the blood group reactivity, only with porphyrin levels that are slightly increased in red cells and decreased in serum. This mild phenotype, along with that of the grossly normal *Abcb6*$^{-/-}$ mouse [40], suggests functional compensation by other ABC transporters such as ABCG2. The absence of significant phenotypic alteration in ABCB6 loss-of-function models demonstrates that hypomorphic and null mutations of ABCB6 expression are of only modest pathological import under unstressed conditions. In contrast, stable structural abnormalities of ABCB6, as in ocular coloboma (incomplete closure of the optic fissure) and FP, cause divergent phenotypes. The ocular coloboma mutations likely decrease ABCB6 function, as suggested by Wang [38]. The ABCB6 mutations of ocular coloboma preferentially affect the eyes, perhaps reflecting the importance of ABCB6 functions in mitochondria and other intracellular organelles especially important to the high-energy requirements and oxidative stress in cells of the eye. In contrast, mature RBCs lack mitochondria, following their autophagic removal in the final stages of erythroid differentiation [38,46].

Conclusions

In conclusion, FP is very likely caused by dominant ABCB6 mutations that appear to be gain-of-function mutations causing abnormal loss of K$^+$ from RBCs, more evident at low temperature. Ongoing functional analysis in ery-

throid cells and in animal models should further elucidate the pathogenic mechanisms of ABCB6 mutations in FP.

Acknowledgments

The authors thank Prof. Gordon W. Stewart (University of College London) for referring families Falkirk and East London, and the CEINGE Service Facility platforms including the Dynamic Imaging Facilities (particularly Dr. Daniela Sarnataro for providing helpful technical support), the Sequencing Core, and the FACS Core Laboratory, directed by Prof. Luigi Del Vecchio. The authors also thank Dr. Faouzi Baklouti for helpful support, and Dr. David Vandorpe for helpful discussion.

Author Contributions

I.A., S.L.A., J.D., and A.I. designed and conducted the study, and prepared the manuscript; C.B., B.E.S., and L.DF. contributed to the preparation of the manuscript; C.A. performed the Western blotting analysis and sequencing analysis; R.R. designed and conducted the selection and sequencing analysis; R.A. and A.K.S. performed the three-dimensional structure modeling and analysis; M.R.E. performed the immunofluorescence analysis.

References

1. Stewart GW, Corrall RJ, Fyffe JA, et al. Familial pseudohyperkalemia. A new syndrome. Lancet 1979;2:175–177.
2. Dagher G, Vantyghem MC, Doise B, et al. Altered erythrocyte cation permeability in familial pseudohyperkalemia. Clin Sci (Lond) 1989;77:213–216.
3. Vantyghem MC, Dagher G, Doise B, et al. [Pseudo-hyperkalemia. Apropos of a familial case]. Ann Endocrinol (Paris) 1991;52:104–108.
4. Haines PG, Crawley C, Chetty MC, et al. Familial pseudohyperkalemia Chiswick: A novel congenital thermotropic variant of K and Na transport across the human red cell membrane. Br J Haematol 2001;112:469–474.
5. Carella M, d'Adamo AP, Grootenboer-Mignot S, et al. A second locus mapping to 2q35-36 for familial pseudohyperkalemia. Eur J Hum Genet 2004;12: 1073–1076.
6. Bruce LJ, Ring SM, Ridgwell K, et al. South-east asian ovalocytic (SAO) erythrocytes have a cold sensitive cation leak: Implications for in vitro studies on stored SAO red cells. Biochim Biophys Acta 1999;1416:258–270.
7. Grootenboer S, Schischmanoff PO, Laurendeau I, et al. Pleiotropic syndrome of dehydrated hereditary stomatocytosis, pseudohyperkalemia, and perinatal edema maps to 16q23-q24. Blood 2000;96:2599–2605.
8. Fricke B, Jarvis HG, Reid CD, et al. Four new cases of stomatin-deficient hereditary stomatocytosis syndrome: Association of the stomatin-deficient cryohydrocytosis variant with neurological dysfunction. Br J Haematol 2004;125: 796–803.
9. Stewart GW. Hemolytic disease due to membrane ion channel disorders. Curr Opin Hematol 2004;11:244–250.
10. Bruce LJ, Robinson HC, Guizouarn H, et al. Monovalent cation leaks in human red cells caused by single amino-acid substitutions in the transport domain of the band 3 chloride-bicarbonate exchanger, AE1. Nat Genet 2005;37:1258–1263.
11. Stewart AK, Vandorpe DH, Heneghan JF, et al. The GPA-dependent, spherostomatocytosis mutant AE1 E758K induces GPA-independent, endogenous cation transport in amphibian oocytes. Am J Physiol Cell Physiol 2010; 298:C283–C297.
12. Bruce LJ, Guizouarn H, Burton NM, et al. The monovalent cation leak in overhydrated stomatocytic red blood cells results from amino acid substitutions in the Rh-associated glycoprotein. Blood 2009;113:1350–1357.
13. Stewart AK, Shmukler BE, Vandorpe DH, et al. Loss-of-function and gain-of-function phenotypes of stomatocytosis mutant RhAG F65S. Am J Physiol Cell Physiol 2011;301C1325–1343.
14. Weber YG, Storch A, Wuttke TV, et al. GLUT1 mutations are a cause of paroxysmal exertion-induced dyskinesias and induce hemolytic anemia by a cation leak. J Clin Invest 2008;118:2157–2168.
15. Bogdanova A, Goede JS, Weiss E, et al. Cryohydrocytosis: Increased activity of cation carriers in red cells from a patient with a band 3 mutation. Haematologica 2010;95:189–198.
16. Flatt JF, Guizouarn H, Burton NM, et al. Stomatin-deficient cryohydrocytosis results from mutations in SLC2A1: A novel form of GLUT1 deficiency syndrome. Blood 2011;118:5267–5277.
17. Bawazir WM, Gevers EF, Flatt JF, et al. An infant with pseudohyperkalemia, hemolysis, and seizures: Cation-leaky GLUT1-deficiency syndrome due to a SLC2A1 mutation. J Clin Endocrinol Metab 2012;97: E987–E993.
18. Zarychanski R, Schulz VP, Houston BL, et al. Mutations in the mechanotransduction protein PIEZO1 are associated with hereditary xerocytosis. Blood 2012;120:1908–1915.
19. Krishnamurthy PC, Du G, Fukuda Y, et al. Identification of a mammalian mitochondrial porphyrin transporter. Nature 2006;443:586–589.
20. Kiss K, Brozik A, Kucsma N, et al. Shifting the paradigm: The putative mitochondrial protein ABCB6 resides in the lysosomes of cells and in the plasma membrane of erythrocytes. PLoS One 2012;7:e37378.
21. Helias V, Saison C, Ballif BA, et al. ABCB6 is dispensable for erythropoiesis and specifies the new blood group system Langereis. Nat Genet 2012;44: 170–173.
22. Meenaghan M, Follett GF, Brophy PJ. Temperature sensitivity of potassium flux into red blood cells in the familial pseudohyperkalaemia syndrome. Biochim Biophys Acta 1985;821:72–78.
23. Gore DM, Layton M, Sinha AK, et al. Four pedigrees of the cation-leaky hereditary stomatocytosis class presenting with pseudohyperkalaemia. Novel profile of temperature dependence of Na+-K+ leak in a xerocytic form. Br J Haematol 2004;125:521–527.
24. Adzhubei IA, Schmidt S, Peshkin L, et al. A method and server for predicting damaging missense mutations. Nat Methods 2010;7:248–249.
25. Andolfo I, De Falco L, Asci R, et al. Regulation of divalent metal transporter 1 (DMT1) non-IRE isoform by the microRNA Let-7d in erythroid cells. Haematologica 2010;95:1244–1252.
26. Chomczynski P, Sacchi N. Single-step method of RNA isolation by acid guanidinium thiocyanate-phenol-chloroform extraction. Anal Biochem 1987;162: 156–159.
27. Sali A, Potterton L, Yuan F, et al. Evaluation of comparative protein modeling by MODELLER. Proteins 1995;23:318–326.
28. Van Der Spoel D, Lindahl E, Hess B, et al. GROMACS: Fast, flexible, and free. J Comput Chem 2005;26:1701–1718.
28a. Laskowski RA, MacArthur MW, Moss DS, and Thornton JM. PROCHECK: a program to check the stereochemical quality of protein structures. J Appl Cryst 1993;26:283–291.
29. Koradi R, Billeter M, Wuthrich K. MOLMOL: A program for display and analysis of macromolecular structures. J Mol Graph 1996;14:51–55, 29–32.
30. DeGorter MK, Conseil G, Deeley RG, et al. Molecular modeling of the human multidrug resistance protein 1 (MRP1/ABCC1). Biochem Biophys Res Commun 2008;365:29–34.
31. Aller SG, Yu J, Ward A, et al. Structure of P-glycoprotein reveals a molecular basis for poly-specific drug binding. Science 2009;323:1718–1722.
32. Dawson RJ, Locher KP. Structure of a bacterial multidrug ABC transporter. Nature 2006;443:180–185.
33. Zutz A, Gompf S, Schagger H, et al. Mitochondrial ABC proteins in health and disease. Biochim Biophys Acta 2009;1787:681–690.
34. Szakacs G, Annereau JP, Lababidi S, et al. Predicting drug sensitivity and resistance: Profiling ABC transporter genes in cancer cells. Cancer Cell 2004;6:129–137.
35. Kelter G, Steinbach D, Konkimalla VB, et al. Role of transferrin receptor and the ABC transporters ABCB6 and ABCB7 for resistance and differentiation of tumor cells towards artesunate. PLoS One 2007;2:e798.
36. Mitsuhashi N, Miki T, Senbongi H, et al. MTABC3, a novel mitochondrial ATP-binding cassette protein involved in iron homeostasis. J Biol Chem 2000;275: 17536–17540.
37. Tsuchida M, Emi Y, Kida Y, et al. Human ABC transporter isoform B6 (ABCB6) localizes primarily in the Golgi apparatus. Biochem Biophys Res Commun 2008;369:369–375.
38. Wang L, He F, Bu J, et al. ABCB6 mutations cause ocular coloboma. Am J Hum Genet 2012;90:40–48.
39. Weber GJ, Choe SE, Dooley KA, et al. Mutant-specific gene programs in the zebrafish. Blood 2005;106:521–530.
40. Ulrich DL, Lynch J, Wang Y, et al. ATP-dependent mitochondrial porphyrin importer ABCB6 protects against phenylhydrazine toxicity. J Biol Chem 2012;287:12679–12690.
41. Cooper DN, Youssoufian H. The CpG dinucleotide and human genetic disease. Hum Genet 1988;78:151–155.
42. Xi X, Bodnar RJ, Li Z, et al. Critical roles for the COOH-terminal NITY and RGT sequences of the integrin beta3 cytoplasmic domain in inside-out and outside-in signaling. J Cell Biol 2003;162:329–339.
43. Mornon JP, Lehn P, Callebaut I. Molecular models of the open and closed states of the whole human CFTR protein. Cell Mol Life Sci 2009;66:3469–3486.
44. Bareil C, Theze C, Beroud C, et al. UMD-CFTR: A database dedicated to CF and CFTR-related disorders. Hum Mutat 2010;31:1011–1019.
45. Hohl M, Briand C, Grutter MG, et al. Crystal structure of a heterodimeric ABC transporter in its inward-facing conformation. Nat Struct Mol Biol 2012;19: 395–402.
46. Zhang J, Randall MS, Loyd MR, et al. Mitochondrial clearance is regulated by Atg7-dependent and -independent mechanisms during reticulocyte maturation. Blood 2009;114:157–164.
47. Fukuda Y, Aguilar-Bryan L, Vaxillaire M, et al. Conserved intramolecular disulfide bond is critical to trafficking and fate of ATP-binding cassette (ABC) transporters ABCB6 and sulfonylurea receptor 1 (SUR1)/ABCC8. J Biol Chem 2011;286:8481–8492.
48. Polireddy K, Khan MM, Chavan H, et al. A novel flow cytometric HTS assay reveals functional modulators of ATP binding cassette transporter ABCB6. PLoS One 2012;7:e40005.